Cone Penetration Tip Resistance Deconvolution Utilizing Complex Cepstrum Analysis

At the 4th International Symposium on Cone Penetration Testing (CPT'18) a paper was presented on the "Inverse filtering procedure to correct cone penetration data for thin-layer and transition effects". The topic of this paper has great similarities with seismic deconvolution, for which BCE has developed algorithms both for seismic deconvolution and seismic blind deconvolution. Based on that work this technical note will suggest an enhancement to the proposed approach in the paper by utilizing the Complex Cepstrum Analysis (CCA).

Introduction - Cone Penetration Deconvolution Problem (after Boulanger and DeJong, 2018)

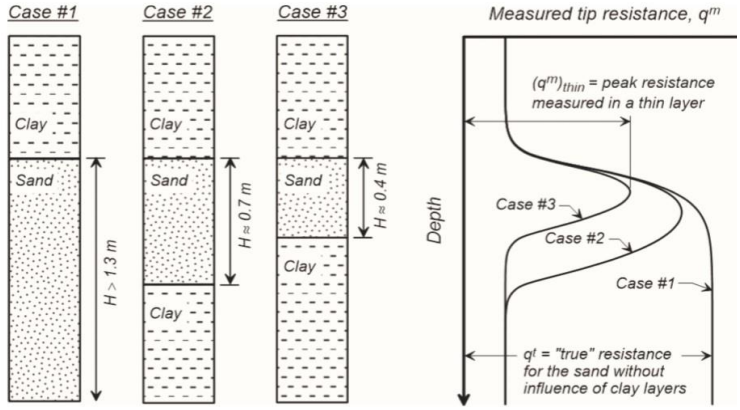

Figure 1. Schematic of thin layer effect for a sand layer embedded in a clay layer (after Boulanger and DeJong, 2018).

When performing a Cone Penetration Test (CPT) layers above and below the cone tip affect the measured tip resistance as illustrated in Figure 1. The measured cone penetration tip resistance q^m can then be described as

$$q^m(z) = q^t(z) * w_c(z) + v(z) \quad (1)$$

where
$q^m(z)$ is the measured cone penetration tip resistance
$q^t(z)$ is the true cone penetration tip resistance
$w_c(z)$ is the "blurring" function
$v(z)$ is additive noise, generally taken to be white with a Gaussian pdf
$*$ is the convolution operation.

Equation (1) can also be represented as

$$q^m(z) = \int_{z_{min}}^{z_{max}} q^t(\tau) w_c(z-\tau) d\tau + v(z) \quad (2)$$

where z_{min} and z_{max} are the limits of the CPT sounding.

The discrete representation of eq. (2) is then

$$q^m(k) \;=\; \sum_{i=1}^{k} q^t(i) w_c\big(k-(i-1)\big) \;+ v(k), \quad k = 1,2\cdots N \tag{3}$$

where N is the length of the depth series.

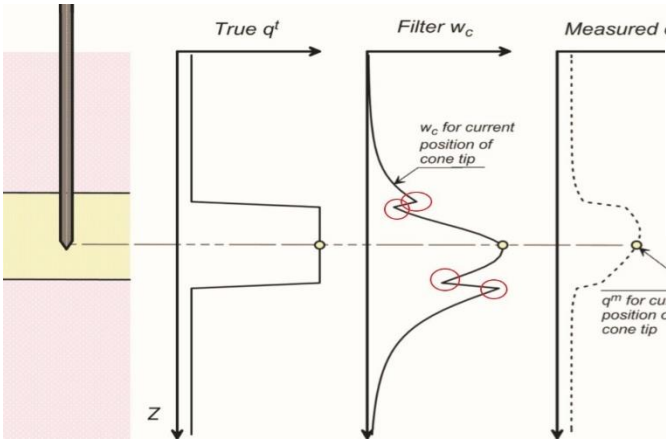

Figure 2. Illustration of the convolution of qt with the cone penetration "blurring" function to obtain q^m at a given point in a layered profile (modified from Boulanger and DeJong, 2018).

Figure 1 illustrates the effect the "blurring" function w_c has on q^t, and in Fig. 2 the convolution of w_c with q^t to give q^m at a given depth is shown. Figure 2 also illustrates the typical form of w_c where the red circles identify sharp points at interfaces which require very high bandwidth frequencies. This w_c feature will be important within the application of CCA as will be outlined below.

Boulanger and DeJong (2018) describe that w_c is depth variant and nonlinear in that it is dependent on q^t, and then utilize the following set of equations to iteratively obtain an estimate of q^t denoted as q^{inv}.

$$dq \;= q^t - q^m \tag{4}$$

$$dq \;= q^t - q^t * w_c(q^t) \tag{5}$$

$$q^t = q^m + dq \tag{6}$$

$$q^t = q^m + (q^t - q^t * w_c(q^t)) \tag{7}$$

$$q_{n+1}^{inv} = q^m + \left(q_n^{inv} - q_n^{inv} * w_c(q_n^{inv})\right) \tag{8}$$

$$err = \frac{\sum\left|(q_{n+1}^{inv} - q_{n+1}^{inv})_i\right|}{\sum|(q^m)_i|} =< \; 10^{-6} \tag{9}$$

Equation (7) is estimated iteratively by implementing eq. (8). In eq. (8), n denotes the n^{th} iteration and $q_1^{inv} = q^m$. The iteration process is continued until the error criterion defined by eq. (9) is met or a maximum number of user specified iterations is reached. In their paper the authors state that this methodology is not well constrained without additional adjustments, and they believe that this is due to the fact that the spatial frequencies are higher than justifiable based on the data sampling interval or physical size of the cone. To address this the authors apply a somewhat ad-hoc smoothing filter followed by a low-pass spatial filter.

In our opinion it is somewhat surprising that the iterative algorithm defined by eq. (8) has been shown to carry out the deconvolution process irrespective of the nonlinearity outlined by eq. (7). We believe this is most likely because $q^t \approx q^m$, which is supported by the fact that $\boldsymbol{q_1^{inv} = q^m}$. For that reason the implementation of eq. (8) would not be possible for seismic deconvolution

where the reflection series is significantly different from the recorded seismogram. The approach for seismic deconvolution as described in the next section also provide an alternate technique for obtaining an estimate of q^t without initializing $q_1^{inv} = q^m$ and based upon the high bandwidth of w_c.

Seismic Deconvolution

In seismology, the measured seismogram s(t) can be described as follows

$$s(t) = b(t) * r(t) + v(t) \tag{10}$$

where
s(t) is the measured seismogram.
b(t) is the seismic wave which is a superposition of earth and instrument responses.
r(t) is the reflectivity of the earth (reflection coefficients).
v(t) is the additive noise, generally taken to be white with a Gaussian pdf.
$*$ denotes the convolution operation.

The primary goal of seismic deconvolution is to remove the characteristics of the source wave from the recorded seismic time series, so that one is ideally left with only the reflection coefficients. These reflection coefficients identify and quantify the impedance mismatches between different geological layers that are of great interest to the geophysicist. Thus the objective is that the source wave is deconvolved from the seismogram, which is the same as that of estimating q^t (i.e., reflection series) by deconvolving w_c (i.e., source wave) from q^m (noisy seismogram) in cone penetration deconvolution. A very challenging and yet common seismic deconvolution problem is where the source wave is unknown and has the potential for time variation. This is referred to as blind seismic deconvolution (BSD) and represents the case where we have one known (measured seismogram with additive noise) and two unknowns (source wave and reflection coefficients).
Seismic deconvolution has been studied extensively and there are many techniques that can be applied to resolve it. The majority of these techniques utilize the steady state Wiener digital filter that assumes a minimum phase source wave, while other techniques implement inverse theory, minimum entropy deconvolution, adaptive deconvolution, principle phase decomposition, and Complex Cepstrum Analysis (CCA). The CCA method is perfectly suitable for situations where the source wave has a high bandwidth as is the case for the "blurring" function w_c in Cone Penetration Tip Resistance Deconvolution (CPTRD). This makes CCA a perfect candidate for incorporation into CPTRD.

Complex Cepstrum Analysis:

The governing equations defining CCA are summarized as below. Using the identity that the convolution operation in the time domain is a multiplication in the frequency domain and taking the frequency transform of eq. (10) (ignoring the noise term) gives

$$S(\omega) = B(\omega)R(\omega) \tag{11}$$

where S(ω), B(ω), and R(ω) are the Fourier transforms of *s(t)*, *b(t)*, and *r(t)*, respectively.

Representing the Fourier transform of the processes in eq. (11) by their magnitudes and phases results in

$$|S(\omega)|e^{\gamma_S(\omega)i} \;=\; |BS(\omega)|e^{\gamma_B(\omega)i} \times |R(\omega)|e^{\gamma_R(\omega)i} \tag{12}$$

where γ(ω) is the phase of the process.

Taking the natural logarithm of both sides of eq. (12) and solving for R(ω) gives

$$Ln|R(\omega)| \;=\; Ln|S(\omega)| - Ln|B(\omega)| \tag{13a}$$

$$\gamma_R(\omega) \;=\; \gamma_S(\omega) - \gamma_B(\omega) \tag{13b}$$

In CCA, eqs. (13a) and (13b) are applied on the recorded seismogram (*s(t)*) and known source wave (*b(t)*) to give the frequency spectrum of the reflection series (*R(ω)*). The inverse Fourier transform is then applied on *R(ω)* to give the desired reflection series (*r(t)*).

To illustrate this process a simulated zero phase Klauder source wave (Vibroseis type source wave) is shown in Fig. 3(a) with the wave's bandwidth of 4 - 140Hz shown in Fig. 3(b). The Klauder source wave is then convolved with the reflection series illustrated in Fig. 4(a) to give the output in Fig. 5. Applying eqs. 13(a) and 13(b) on the output shown in Figs. 3(a) and 5(a) and taking the inverse Fourier transform generates the outcome shown in Fig. 6, which reflects that the reflection series is recovered accurately. Finally Fig. 7 illustrates the frequency ratio between seismogram and source wave.

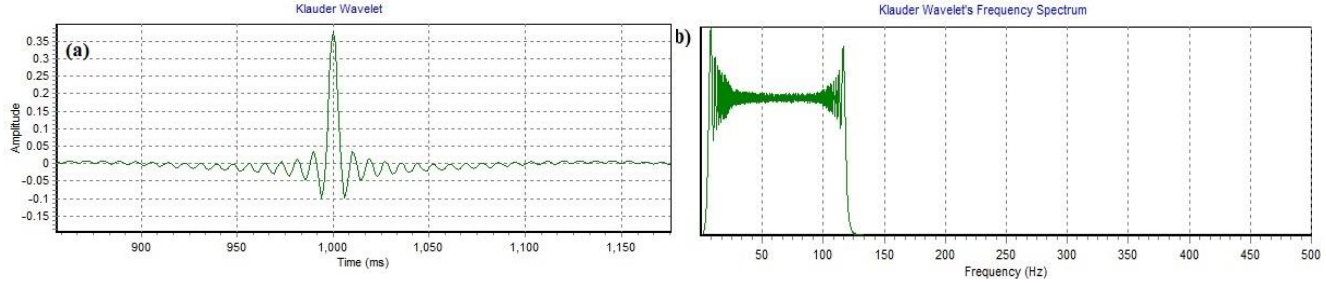

Figure 3. Simulation of the zero phase Klauder source wave (a) and corresponding frequency spectrum (b).

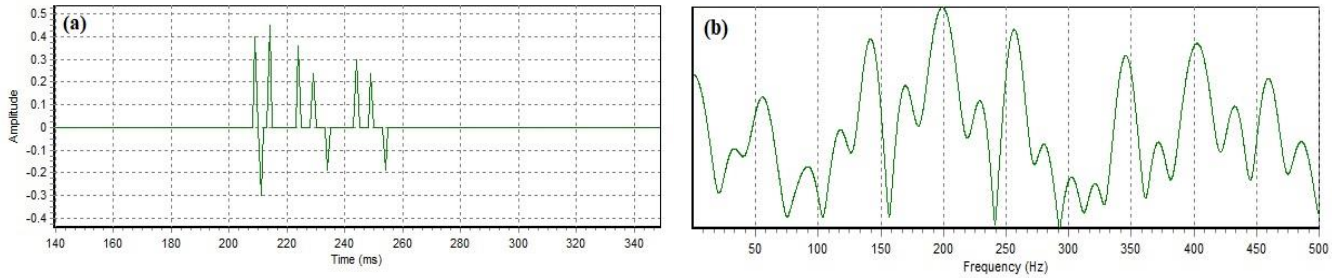

Figure 4. Reflection series (a) and corresponding frequency spectrum (b).

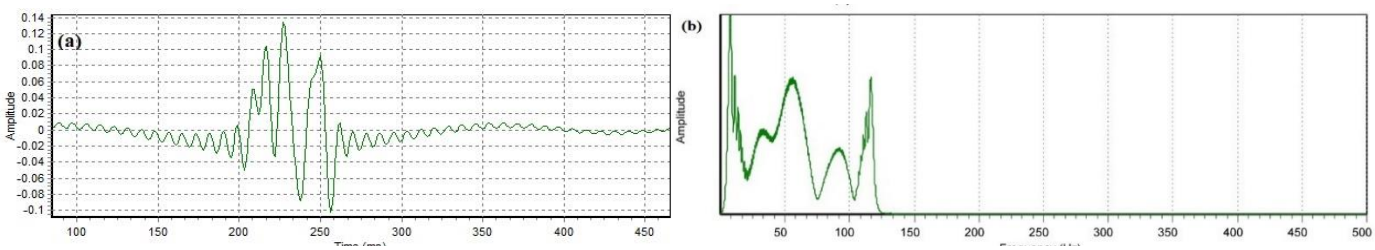

Figure 5. Simulated seismogram (a) and corresponding frequency spectrum (b).

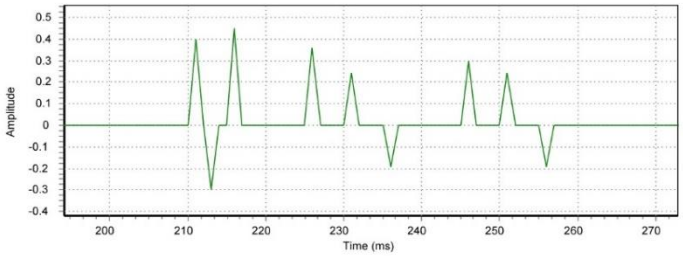

Figure 6. CSA estimated reflection series.

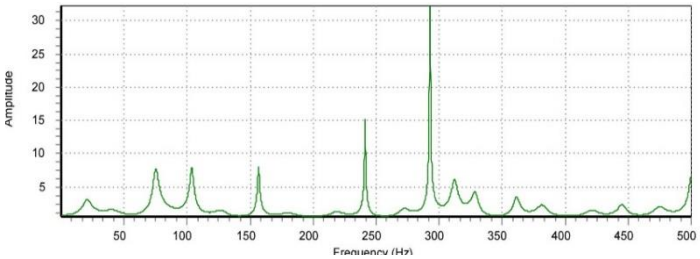

Figure 7. Frequency spectrum ratio between source wave of Fig 3(a) and seismogram of Fig. 5(a).

The CCA works ideally in deconvolution if the seismogram is noise free, which is obviously not the case, and therefore eq. (11) to 13(a) are updated below to reflect measurement noise.

$$S(\omega) = B(\omega)R(\omega) + V(\omega) \tag{14}$$

$$S(\omega) = B(\omega)R(\omega)(1 + V(\omega)/B(\omega)R(\omega)) \tag{15}$$

$$Ln|Z(\omega)| = Ln|B(\omega)| + Ln|R(\omega)| + Ln\left|1 + V(\omega)/\left(B(\omega)R(\omega)\right)\right| \tag{16}$$

$$Ln|R(\omega)| = Ln|S(\omega)| - Ln|B(\omega)| - Ln\left|1 + V(\omega)/\left(S(\omega)R(\omega)\right)\right| \tag{17}$$

With measurement noise the performance of CCA is directly dependent upon the frequency ratio of the source wave to the seismogram. The reflection series is a high bandwidth signal (see Fig. 4(b)) and that means that if the frequencies outside of the source wave's bandwidth (e.g., 4 Hz to 120 Hz (as shown in Fig. 3(b)) are negligible, then the CCA cannot estimate the reflection series *r(t)*. This is evident from the last term in eq. (17) (i.e., $Ln\left|1 + V(\omega)/\left(S(\omega)R(\omega)\right)\right|$). For example, Fig. 7 illustrates the Klauder source wave / seismogram frequency ratio without noise present in the seismogram, which indicates that there is measurable Klauder source wave to seismogram frequency information for all frequencies within the Nyquist. Figure 8(a) shows the seismogram of Fig. 5(a) with a small amount of measurement noise added, and Fig. 8(b) then gives the associated frequency ratio of the source wave / seismogram.

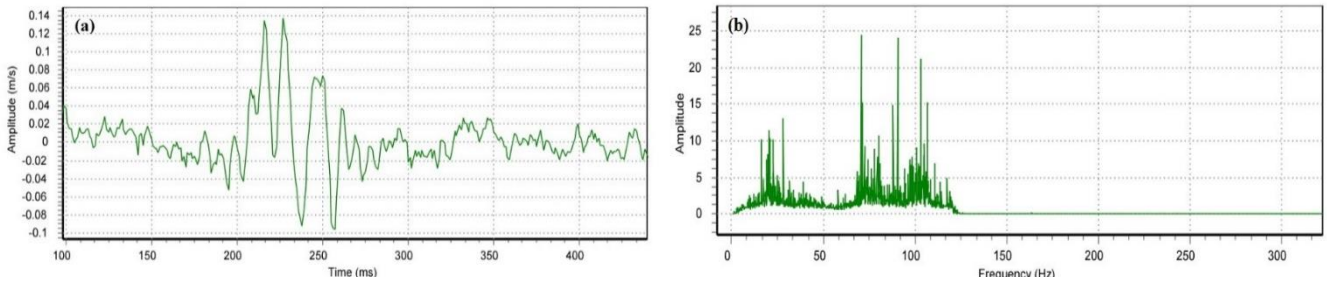

Figure 8. (a) Simulated seismogram of Fig 5(a) with measurement noise added. (b) Frequency spectrum ratio between source wave of Fig 3(a) and seismogram of Fig. 8(a).

As is shown in Fig. 8(b), there is hardly any frequency information above 120 Hz, simply because the Klauder source had minimal signal information outside of the frequency band of 4 Hz to 120 Hz. Implementing CCA on the seismogram of Fig. 8(a) would results in the nonsensical reflection series estimates as illustrated in Fig. 9. If on the other hand the source wave had significant frequency information for frequencies ranging from 0 Hz to the Nyquist (resulting in a broadband source wave / seismogram frequency ratio), then the CCA would produce desirable results. To illustrate this a one-sided Klauder source wave is shown in Fig. 10(a), and the sharpness of the peak response requires a large bandwidth of frequencies as is illustrated in Fig. 10(b). The resulting CCA estimate for this data set is then given in Fig. 11. Comparing Fig. 11 and 6, it is evident that there is very good agreement with the true reflection series.

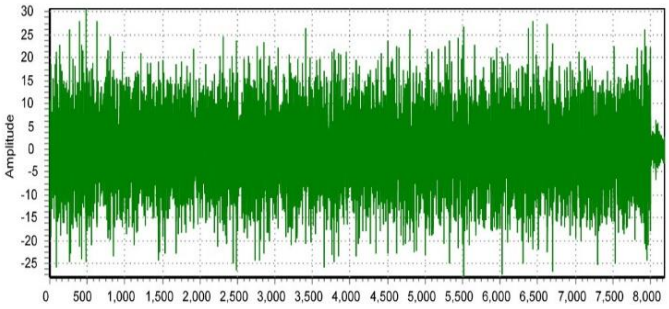

Figure 9. CSA estimated reflection series when measurement noise present.

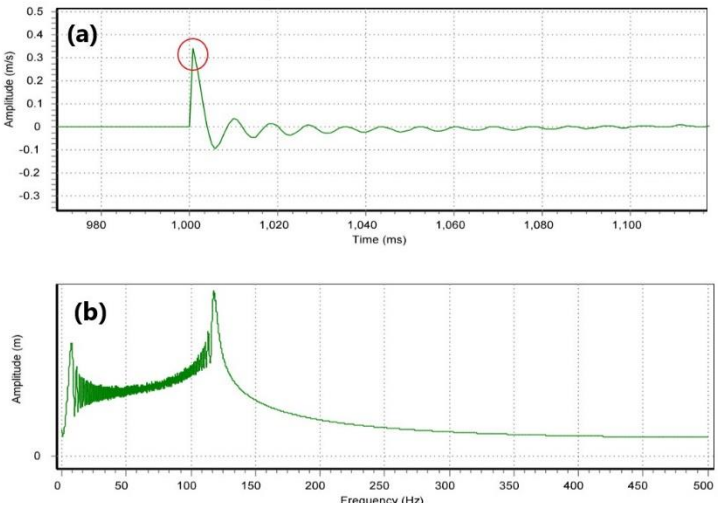

Figure 10. Simulation of the one-sided Klauder source wave (a) and corresponding frequency spectrum (b).

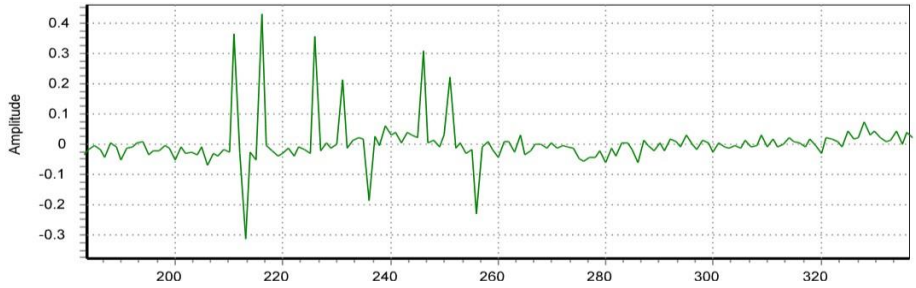

Figure 11. CSA estimated reflection series from seismogram generated with a one side Klauder source wave and the reflection series illustrated in Figs. 4 and 6.

Estimating q^t with CCA:

The form of the cone penetration "blurring" function w_c is ideally suited for CCA as was illustrated in Fig. 2. This figure illustrated the typical form of w_c where the red circles identified sharp points at interfaces, similar to the one shown in Fig. 10a, which require very high bandwidth frequencies.

Consequently eq. 14 – 17 can be easily adopted for CPT cone bearing deconvolution by making the following substitutions:

$q^m \rightarrow s(t)$, $w_c \rightarrow b(t)$, $r(t) \rightarrow q^t$, $Q^m(\omega) \rightarrow S(\omega)$, $W_c(\omega) \rightarrow B(\omega)$, and $R(\omega) \rightarrow Q^t(\omega)$.

The proposed CCA algorithm for estimating q^t from q^m and $w_c(q^t)$ is outlined below where eq. (8) is updated to take into account a direct estimate of q^t when initializing the estimation iteration of eq. (8). In this case $q_1^{inv} = q^t(z)$ where is calculated using eqs. (18), (19) and (20). For each subsequent iteration (i.e., $n = n+1$), $w_c(q^t, z)$ is calculated utilizing the previous estimate of q^{inv} (i.e., $w_c(z, q_{n-1}^{inv})$) and a new estimate of q_{n+1}^{inv} is obtained. This iteration process is continued until the error criterion defined by eq. (9) is met or a maximum number of user specified iterations is reached. It is also foreseen that a parameter estimation component could be incorporated into the CPTRD so that the w_c model parameters (e.g., m_z and m_q) could also be refined.

$$q^m(z) = q^t(z) * w_c(z) + v(z) \quad (1)$$

$$err = \frac{\sum \left| \left(q_{n+1}^{inv} - q_{n+1}^{inv}\right)_i \right|}{\sum |(q^m)_i|} =< 10^{-6} \quad (9)$$

$$Q^m(\omega) = F(q^m) \quad (18a)$$

$$Q^t(\omega) = F(q^t) \quad (18b)$$

$$W_c(\omega) = F(w_c) \quad (18c)$$

$$Ln|Q^t(\omega)| = Ln|Q^m(\omega)| - Ln|B(\omega)| \quad (19a)$$

$$\gamma_{Q^t}(\omega) = \gamma_{Q^m}(\omega) - \gamma_{w_c}(\omega) \quad (19b)$$

$$q^t(z) = F^{-1}\left(Q^t(\omega)\right) \quad (20)$$

where F denotes the Fourier transform and F^{-1} denotes the inverse Fourier transform

April 29, 2020 Update:

After extensive analysis and implementation of the equations outlined in the referenced paper it was determine that the convolution operation (equations (1), (2), (10), (12) and (13) of referenced paper) was not applied. Instead a simple sum weighted window is implemented. In this approach the blurring function w_c is not convolved with *qt* but it simply is multiplied with w_c over the w_c window length.

$$q_m(i) = \sum_{j=1}^{60*\left(\frac{d_c}{\Delta}\right)} w_c(j) \times q_t(\Delta_{qt} + j)$$

$$\Delta_{qt} = (i - \Delta_{wc}), \quad \Delta_{wc} = 30 * \left(\frac{d_c}{\Delta}\right) \tag{21}$$

Δ is the q_t depth sampling rate

Clearly since there isn't a convolution applied to *qt* - any deconvolution algorithm will not work and CCA is not applicable. BCE is going to instead implement a Particle Filter (PF) type formulation to address the challenging problem of extracting *qt* from *qm*. This PF formulation will be similar to the algorithm outlined in Baziw, E. and Verbeek, G. (2012), "Passive (Micro-) Seismic Event Detection by Identifying Embedded "event" Anomalies within Statistically Describable Background Noise", Pure appl. geophys., vol. 169, Issue 12, pp 2107-2126.

Erick Baziw
Gerald Verbeek